Research Article Vol. 29, No. 24 / 22 Nov 2021 / Optics Express 39065

Optics EXPRESS

Generalized polarization transformations with metasurfaces

AUN ZAIDI,[1,3] NOAH A. RUBIN,[1] AHMED H. DORRAH,[1] JOON-SUH PARK,[1,2] AND FEDERICO CAPASSO[1,4]

[1]*Harvard John A. Paulson School of Engineering and Applied Sciences, Harvard University, Cambridge, Massachusetts 02138, USA*
[2]*Nanophotonics Research Center, Korea Institute of Science and Technology, Seoul 02792, Republic of Korea*
[3]*zaidi01@g.harvard.edu*
[4]*capasso@seas.harvard.edu*

Abstract: Metasurfaces are arrays of sub-wavelength spaced nanostructures, which can be designed to control the many degrees-of-freedom of light on an unprecedented scale. In this work, we design meta-gratings where the diffraction orders can perform general, arbitrarily specified, polarization transformation without any reliance on conventional polarization components, such as waveplates and polarizers. We use matrix Fourier optics to design our devices and introduce a novel approach for their optimization. We implement the designs using form-birefringent metasurfaces and quantify their behavior – retardance and diattenuation. Our work is of importance in applications, such as polarization abberation correction in imaging systems, and in experiments requiring novel and compact polarization detection and control.

1. Introduction

Polarization is the path of oscillation of light's electric field, which directly follows from the plane-wave solution to Maxwell's equations [1–3]. Polarization of light has played a critical role in the advancement of science and technology, even before the concept was well understood. A well studied example from history, of the exploitation of polarization in primitive technology, is that of the use of calcite crystals as 'sun stones' by the Vikings back in the seventeenth century, for navigation [4]. In the nineteenth and twentieth centuries, polarization of light and polarization-based effects were rigorously studied and developed by many brilliant scientists including Malus (Malus' Law), Brewster (Brewster's angle), Fresnel (Fresnel coeffecients), Stokes (Stokes calculus), Maxwell (Maxwell's equations), and Jones (Jones calculus) [5]. A thorough understanding, and a robust framework delivered through these efforts in the study of polarization, have since contributed to a myriad of inventions and innovations in science and technology, including in fiber-optic based telecommunications [6,7], in astrophysics and astro-imaging [8,9], chemical sensing and characterization [10–12], medicine [11,12], polarization-resolved imaging [13,14], quantum light-matter interaction [15], and quantum information science [16,17], to list a few.

Traditionally – and quite ubiquitously in optical labs – polarization is manipulated using bulk optics such as polarizers and waveplates. Recent advances in nanotechnology [18–20], however, have provided an opportunity to revisit and reinvent the design space for polarization optics, to achieve unprecedented, wavelength-scale control over the polarization properties of an optical system. One such recent advance in nanotechnology – which is also our technology of choice for this work – is known as a metasurface, which is a subwavelength array of artificially engineered nanopillars [20–22]. Recent research in polarization optics involving metasurfaces include examples such as polarization beam splitters [22,23], chiral lenses [24,25], polarization generation diffraction gratings [26,27], and polarization vectorial holograms [28,29]. These, and

#442844 https://doi.org/10.1364/OE.442844
Journal © 2021 Received 12 Sep 2021; revised 18 Oct 2021; accepted 20 Oct 2021; published 8 Nov 2021

Optics EXPRESS

similar works, assume a particular incident polarization-vector for their designs, which essentially restricts the design space available for the most general polarization transformations. We, instead, use the matrix Fourier optics formalism [30], with a gradient descent based optimization, to design the most general polarization (Jones) matrix transformations in the far-field. Using dielectric metasurfaces, we implement two-dimensional diffraction gratings that behave as multi-order polarizing element devices with user-defined polarization properties in chosen diffraction orders. The proposed design principle in our work is general enough that it can be used to design any set of arbitrary polarization transformations in the far-field. We show practical implementation of our optimized designs using dielectric metasurfaces, as proof of principle. Despite recent progress [31–33], our work is the first such design and implementation of an optical device that has simultaneous and complete control over the polarization transformation properties of resulting diffraction orders in the far-field, of a fully polarized system (i.e. no depolarization). Our work bridges the gap that exists in solutions to problems involving compact and precise polarization control, such as the correction of polarization abberations in optical systems [34].

1.1. Description of polarization transformation properties

In the context of this work, assume no depolarization. In that case, polarized light can be represented as a two-dimensional vector, commonly known as a Jones vector:

$$|j\rangle = Ae^{i\varphi}\begin{pmatrix} 1 \\ \alpha e^{i\Delta\phi} \end{pmatrix} \tag{1}$$

where A is the overall amplitude and φ is the overall phase, of the EM wave, while α and $\Delta\phi$ are the relative amplitude and relative phase respectively, between x-polarized and y-polarized light. α and $\Delta\phi$ are usually of more significance in polarization optics, because they fully describe the state of polarization. The Jones vector in an optical system can be transformed – completely – by a 2×2 complex matrix called the Jones matrix, $\boldsymbol{J}$. In practice, it is often useful to decompose an arbitrary Jones matrix transformation, into a product of two sub-transformations: the ‘retarder’ transformation that transforms the global and relative phases of the Jones vector, and the ‘diattenuator’ transformation, that transforms the global and relative amplitudes of the Jones vector. Mathematically, the Jones matrix can be decomposed using the polar decomposition into the product of a unitary matrix $\boldsymbol{U}$, and a Hermitian matrix $\boldsymbol{H}$.

$$\boldsymbol{J} = \boldsymbol{U}\boldsymbol{H} \tag{2}$$

In the context of polarization optics then, $\boldsymbol{U}$ is equivalent to the ‘retarder’ transformation (Fig. 1(a)), and $\boldsymbol{H}$ is equivalent to the ‘diattenuator’ transformation (Fig. 1(b)).

Note that a ‘retarder’, being unitary, has phase-only eigenvalues. Phases (ϕ_1, ϕ_2) of the complex eigenvalues (u_1, u_2) of $\boldsymbol{U}$ are used to define the retardance as:

$$R = |\phi_1 - \phi_2|, \qquad 0^\circ \leq R \leq 180^\circ \tag{3}$$

The generally complex, and orthogonal eigenvectors $(\vec{r_1}, \vec{r_2})$ corresponding to the eigenvalues (u_1, u_2) are known as the retardance axes. A light wave polarized along $\vec{r_1}$ would accumulate R° more phase compared to a light wave polarized along $\vec{r_2}$. A common example of a ‘retarder’ would be a quarter-wave plate (QWP), with $R = 90^\circ$, and eigen-axes parallel to the fast and slow axes of the QWP.

Now, a ‘diattenuator’, being Hermitian, has only real eigenvalues. The eigenvalues (t_1, t_2) of $\boldsymbol{H}$, and the eigenvectors are used to define the ‘diattenutation’ property of the polarization

Optics EXPRESS

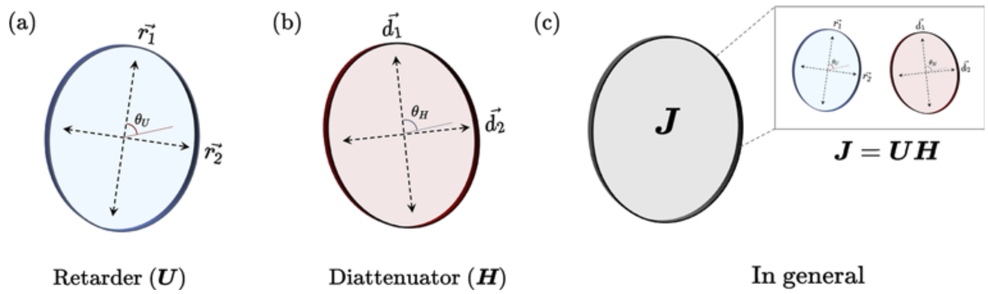

Fig. 1. Jones matrix decomposition. (a) A unitary transformation, $\boldsymbol{U}$, which satisfies $\boldsymbol{U}^\dagger \boldsymbol{U} = \mathbb{I}$, is a lossless transformation. Plane-waves incident along eigenvectors $(\vec{r}_1, \vec{r}_2)$, will generally accumulate separate phases. Physically, a retarder or a waveplate can perform a unitary Jones matrix transformation. (b) A Hermitian transformation, $\boldsymbol{H}$, satisfies $\boldsymbol{H}^\dagger = \boldsymbol{H}$. Plane-waves incident along eigenvectors $(\vec{d}_1, \vec{d}_2)$, will generally transmit with different amplitudes. Physical implementation of a Hermitian Jones matrix is known as a diattenuator, a limiting case of which is known as a polarizer. (c) In general, any arbitrary 2×2 Jones matrix $\boldsymbol{J}$ can be written as a cascade of a diattenuator ($\boldsymbol{H}$), followed by a retarder ($\boldsymbol{U}$).

transformation. The diattenutation D of a polarization transformation is defined as:

$$D = \frac{|t_1|^2 - |t_2|^2}{|t_1|^2 + |t_2|^2}, \qquad 0 \leq D \leq 1 \tag{4}$$

The generally complex, and orthogonal eigenvectors $(\vec{d}_1, \vec{d}_2)$ corresponding to the eigenvalues (t_1, t_2) are known as the diattenuation axes. Note that t_1 and t_2 are transmission amplitudes for light wave polarized along $\vec{d}_1$ and $\vec{d}_2$, respectively. The diattenuation D, then, tells us the contrast in transmission, between polarized light along $\vec{d}_1$ and $\vec{d}_2$. A common example of a 'diattenutator' would be an ideal linear polarizer, with $D = 1$, and diattenuation-axes parallel to the maximum/minimum transmission axes of the polarizer.

In an optical system, even if the resulting polarization transformation is a mixture of retardance and diattenuation, it can always be decomposed into its unitary and Hermitian parts using Eq. (2), so that the retardance and diattenuation properties can be studied in isolation (Fig. 1). In our work, by showing complete control over the retardance and diattenutation properties in the design space of our optimization, we design and fabricate devices that can perform the most general polarization transformations allowed by our metasurface platform.

2. Materials and methods

2.1. Matrix Fourier optics

In design, what enables us to have complete access to the retardance and diattenutation properties, in the far-field, is a recently developed theory [30] known as 'Matrix Fourier optics'. It is the matrix generalization – which is allowed due to the linearity of the system – of the well established Fourier optics, that links the 'near-field' (ignoring evanescent waves) to the far-field, by a simple Fourier transform, as physically depicted in Fig. 2(a). In case of matrices, the coefficients in the Fourier integral are not scalars, but instead are matrices, and we can write the modified Fourier integral as:

$$\tilde{\boldsymbol{J}}(k_x, k_y) = \iint_{-\infty}^{+\infty} \boldsymbol{J}(x, y) e^{-i(k_x x + k_y y)} dxdy \tag{5}$$

where $\tilde{\boldsymbol{J}}(k_x, k_y)$ is a distribution of 2×2 Jones matrices in the far-field over angular coordinates (k_x, k_y), whereas $\boldsymbol{J}(x, y)$ is a distribution of 2×2 Jones matrices in the plane of incidence, over

Optics EXPRESS

spatial coordinates (x, y). Note that the Fourier integral is distributed across each of the four elements of $\boldsymbol{J}(x, y)$, yielding a matrix Fourier coefficient $\tilde{\boldsymbol{J}}(k_x, k_y)$.

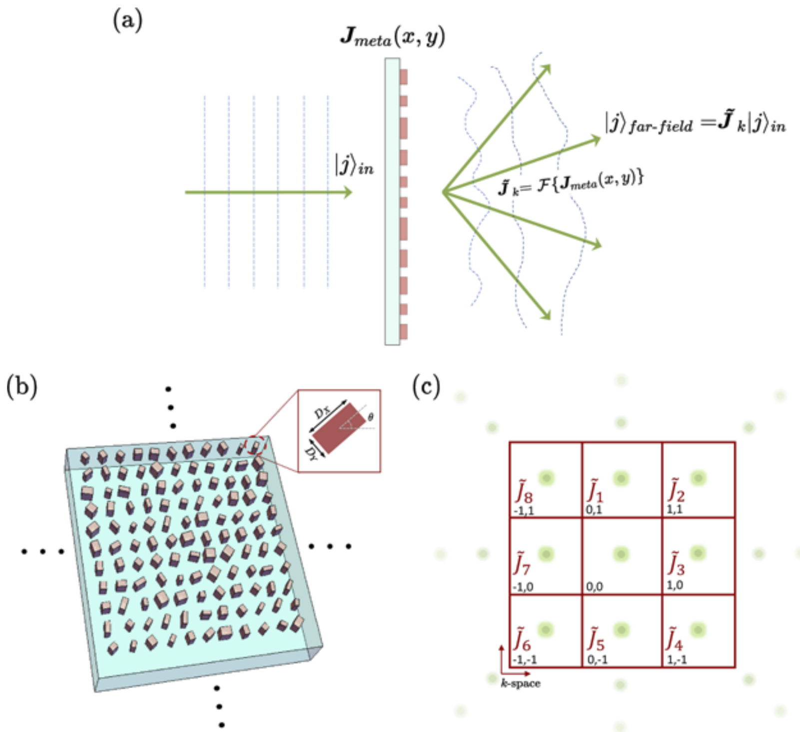

Fig. 2. Metasurface design using Matrix Fourier optics. (a) A specially designed metasurface with Jones matrix distribution $\boldsymbol{J}_{meta}(x, y)$, has plane-wave polarization response $\boldsymbol{J}_k$ in the far-field. (b) Representation of a single period of a 2D metasurface diffraction grating, made up of discrete form-birefringent nanopillars. Each nanopillar within a period, offers 3 independent degrees of freedom: propagation phases ϕ_X and ϕ_Y (controlled by the length D_X and width D_Y) and geometric phase controlled by the relative angular orientation θ. (c) Representation of the far-field discrete diffraction orders, where the desired orders are engineered to have specific polarization transforming properties. If light is incident on the metasurface with some polarization $|j\rangle_{in}$, then the output in order $(0, 1)$ will be $\tilde{\boldsymbol{J}}_1|j\rangle_{in}$, in order $(1, 1)$ will be $\tilde{\boldsymbol{J}}_2|j\rangle_{in}$, and so on.

This calculus forms the basis of our work, and enables us to set up an optimization to realize arbitrary polarization transformations in the far-field, as detailed next.

2.2. Design principle

Let us consider a diffraction grating with chosen orders of diffraction with reasonably high efficiencies, that performs desired polarization transformations for light diffracted in those orders. To design such a grating, we can write the Matrix Fourier series which follows from Eq. (5):

$$\boldsymbol{J}_{meta}(x, y) = \sum_{\vec{k}\epsilon\{G\}} \tilde{\boldsymbol{J}}_k e^{i(k_x x + k_y y)} \tag{6}$$

Equation (6) gives us a straightforward relation to finding the appropriate spatially varying Jones matrix distribution $\boldsymbol{J}(x, y)$ in the incident plane, to get a set of desired Jones matrices $\tilde{\boldsymbol{J}}_k$ in the far-field. However, practically speaking, we are constrained when it comes to implementing

$\boldsymbol{J}(x, y)$ because metasurfaces, consisting of shape birefringent optical elements, can only perform unitary and symmetric transformations at the plane of incidence, of the form:

$$\boldsymbol{J}_{meta}(x, y) = R(\theta(x, y))\begin{pmatrix} e^{i\phi_X(x,y)} & 0 \\ 0 & e^{i\phi_Y(x,y)} \end{pmatrix}R(-\theta(x, y)) \tag{7}$$

where $R(\theta)$ is the 2×2 rotation matrix. ϕ_X and ϕ_Y are the phases imparted on the two orthogonal linear polarizations (X and Y), as incident light propagates through a nanopillar within the metasurface. θ is the orientation of the nanopillar in relation to a reference, and is responsible for introducing geometric phase in our design. In designing a device with far-field Jones matrices $\tilde{\boldsymbol{J}}_k$ in orders of interest ($\vec{k}\epsilon\{G\}$), with reasonably high diffraction efficiencies, while satisfying the form of $\boldsymbol{J}_{meta}(x, y)$ in Eq. (7) at each spatial coordinate (x, y) in the incident plane, we need to setup and run a constrained optimization with respect to a figure of merit. Our optimization of choice is the gradient descent optimization (from the scipy.optimize library in Python), with Lagrange multipliers to handle constraints. Note that $\phi_X(x, y)$, $\phi_Y(x, y)$ and $\theta(x, y)$ can each be independently controlled at each spatial coordinate (x, y) within the metasurface, and provide us with the degrees of freedom to optimize for a particular design.

Consider the design of a two-dimensional diffraction grating where the first eight orders of diffraction $\{G\} = \{(0, 1), (1, 1), (1, 0), (1, -1), (0, -1), (-1, -1), (-1, 0), (-1, 1), (0, 1)\}$ are chosen to produce desired $\tilde{\boldsymbol{J}}_k$ in these diffraction orders, as shown in Fig. 2(a). Note that the choice of orders and $\tilde{\boldsymbol{J}}_k$ is arbitrary and totally designer-specified. To run an optimization to design such a grating using our degrees of freedom $\phi_X(x, y)$, $\phi_Y(x, y)$ and $\theta(x, y)$, in conjunction with Eq. (6) and Eq. (7), we define the following figure of merit to be maximized:

$$\text{Figure of merit: } \sum_{\vec{k}\epsilon\{G\}} Tr(\tilde{\boldsymbol{J}}_k^{\dagger}\tilde{\boldsymbol{J}}_k) \tag{8}$$

The trace $Tr(\tilde{\boldsymbol{J}}_k^{\dagger}\tilde{\boldsymbol{J}}_k)$ is simply the sum of the square of amplitudes of the complex entries in $\tilde{\boldsymbol{J}}_k$, and ensures that the optimization maximizes the diffraction efficiency in the set of orders of interest $\{G\}$.

To get the desired performance in the far-field, we introduce the following two constraints in our optimization:

$$\text{Constraint I: } \sigma\left(Tr(\tilde{\boldsymbol{J}}_k^{\dagger}\tilde{\boldsymbol{J}}_k)\right) = 0 \tag{9}$$

$$\text{Constraint II: } \underbrace{\left|\frac{\vec{\boldsymbol{J}}_k.\vec{\boldsymbol{J}}_{k,des}}{|\vec{\boldsymbol{J}}_k||\vec{\boldsymbol{J}}_{k,des}|}\right|}_{\text{for all } k\epsilon\{G\}} = 1 \tag{10}$$

In Constraint I (Eq. (9)), σ operator computes the standard deviation in the computed traces $Tr(\tilde{\boldsymbol{J}}_k^{\dagger}\tilde{\boldsymbol{J}}_k)$, for all $k\epsilon\{G\}$. We want this standard deviation to be 0, to ensure that the 'weights' of the Jones matrices $\tilde{\boldsymbol{J}}_k$ in the desired orders are uniform; physically, one can think of this in terms of the 'diffraction efficiencies'. (Note, that since the response is polarization dependent, we are defining the diffraction efficiency of an order as the average transmission efficiency of that order for any two orthogonal polarizations.) This constraint essentially helps us avoid the case where one, or more, orders of interest have extremely low efficiencies, because the figure of merit (Eq. (8)) optimizes for the sum total of the efficiencies. Note, however, that the exact diffraction efficiency ratios in Constraint I (Eq. (9)) can be chosen arbitrarily, and that uniform efficiencies is simply one of infinite choices. Constraint II (Eq. (10)) is the constraint in our optimization which ensures that the Jones matrices $\tilde{\boldsymbol{J}}_k$, during the optimization, converge to the desired forms $\tilde{\boldsymbol{J}}_{k,des}$, for all $k\epsilon\{G\}$. To fully understand Constraint II (Eq. (10)), note that we convert each complex-valued 2×2 Jones matrix $\tilde{\boldsymbol{J}}_k$, into an 8-element vector $\vec{\boldsymbol{J}}_k$:

$$\tilde{\boldsymbol{J}}_k = \begin{pmatrix} a_r + ia_i & b_r + ib_i \\ c_r + ic_i & d_r + id_i \end{pmatrix} \Longrightarrow \vec{\boldsymbol{J}}_k = \begin{pmatrix} a_r \\ a_i \\ \vdots \\ d_r \\ d_i \end{pmatrix} \tag{11}$$

This allows us to simply use the vector dot product in Constraint II (Eq. (10)) to ensure that the computed Jones matrices at each iteration, and the desired Jones matrices, are 'aligned' - i.e, have the same form. In summary, the figure of merit (Eq. (8)) ensures that the overall efficiency of the device is as high as possible, while Constraint I (Eq. (9)) ensures that the diffraction efficiencies are uniformly distributed across orders of interest, and Constraint II (Eq. (10)) ensures that the Jones matrices in orders of interest are implemented as desired.

As far as order efficiencies are concerned in the final design, at least currently, it is not possible to predict theoretically what the efficiency might be for some arbitrary grating design (or what the global maximum might be during optimization). It is known that a scalar phase-only grating may only have one or infinitely many diffraction orders [35], and so a grating which is phase-only can never be a solution to an arbitrary beam-splitter design (in which all the light is diffracted into a limited and finite set of orders). Extending this scalar analogy to the case of Jones matrix gratings, we have shown previously [30] that a unitary only grating (Eq. (7)) can never be a solution to an arbitrary beam-splitter design, of the types we show in this work (so we know the theoretical efficiency would be less than 100%). Therefore, the purpose of the optimization is to converge to a local maximum with a high enough efficiency for our application of choice. In designs in Figs. 4–6, we report numerical diffraction efficiencies as high as 77%. In each of the examples shown in Figs. 4–6, the optimization took roughly 3 hours to converge, using a 16 GB RAM, core i7 CPU with 1.80GHz processor.

2.3. Device fabrication and characterization

Using the design principle and techniques described above, we design a range of polarization controlling 2D metasurface diffraction gratings, as proof of concept. We stress that the design choices are arbitrary, and that in practice, these gratings can be designed to suit desired applications in polarization optics, some of which we discuss later in the **Discussion** section.

Once the designs are ready, and we have the required values of our parameters $\phi_X(x,y)$, $\phi_Y(x,y)$ and $\theta(x,y)$ at each lattice point within a period on our metasurface diffraction grating (note that spatial coordinate (x,y) are descritized as seen in Fig. 2(b)), we can select the appropriate pillar (planar) dimensions from a library of simulated pillar results, using the scheme described in [22]. We prepare our device for fabrication by first spin coating a fused silica substrate with a positive tone electron beam resist, with the appropriate thickness (pillar height). After baking, the pillar patterns are written by exposing the resist using electron beam lithography. The developed pattern defines the geometry of the individual nanopillars. Afterwards, we deposit TiO_2 using atomic layer deposition (ALD), to conformally coat the developed pattern. The excess layer of TiO_2 on top of the device is etched away by reactive ion etching (RIE). We finally remove the resist chemically, leaving the desired TiO_2 nanopillars, on top of the substrate, surrounded by air. The fabrication process is described in much greater detail in Ref. [20]. The SEM images of one of the fabricated metasurface gratings are shown in Fig. 3.

The diffraction gratings are measured and characterized using the setup shown in Fig. 3(a). Given that commercial half-wave plates (HWPs) and quarter-wave plate (QWPs), can sometime

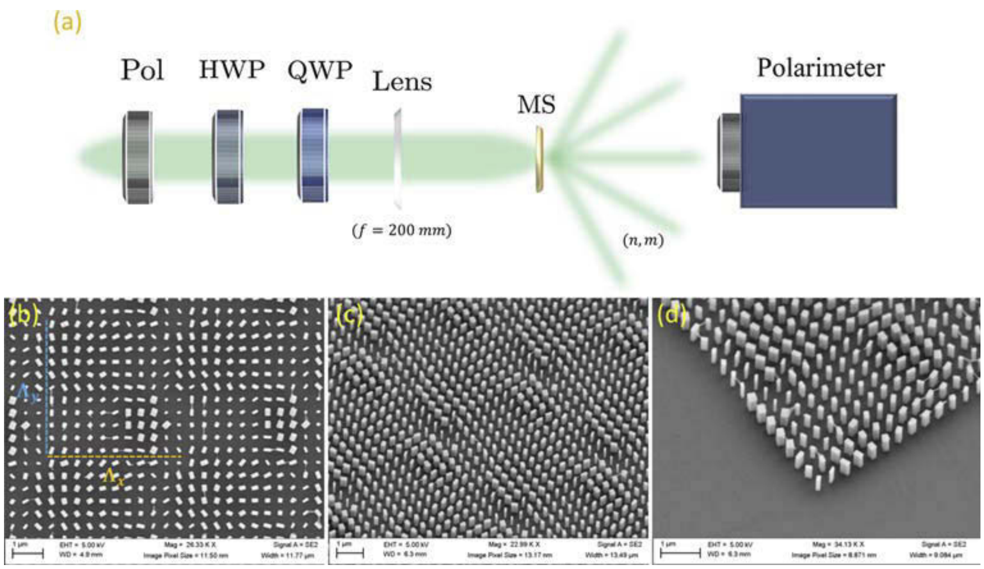

Fig. 3. Measurement setup and SEM images. (a) The incident polarization states are prepared by using a polarizer, half-wave plate (HWP), and quarter-wave plate (QWP), which are mounted on automated rotational stages. A long focal length lens is used to reduce the spot size, without introducing any significant higher-k components. The polarized light is incident on the metasurface sample (MS), and the resulting diffraction orders are measured one by one, by using a commercial polarimeter mounted on a custom 3D rotating mount. (b) Top-view of a fabricated metasurface grating. The periods Λ_x and Λ_y, in x and y spatial directions respectively, both equal 4.62μm, consisting of 11 nanopillars in each direction, uniformally spaced by 420nm. (c) Slightly angular top-view of a metasurface diffraction grating, showing sidewalls of the nanopillars. (d) Angular top-view of the edge of a metasurface diffraction grating. All nanopillars have a constant height of 600nm.

have a significant error in retardance, and are also sensitive to incidence angle, it is important to perform the measurements using a calibrated procedure. We first perform a calibration using K pairs of HWP and QWP orientations. ($K = 16$ was found sufficient in our case.) The polarizations generated by these orientations, which are chosen to adequately sample the Poincaré sphere, are stored in a calibration matrix:

$$\tilde{C} = \begin{pmatrix} | & | & \cdots & | \\ \vec{S}_1^{in} & \vec{S}_2^{in} & \cdots & \vec{S}_k^{in} \\ | & | & \cdots & | \end{pmatrix} \tag{12}$$

The K polarizations are then incident on the metasurface, turn-by-turn, and the Stokes vector output on order (n, m) in response to k^{th} input polarization is recorded as $\vec{S}_k^{(n,m)}$, and all these Stokes vectors are stored in the output matrix:

$$\tilde{O}_{(n,m)} = \begin{pmatrix} | & | & \cdots & | \\ \vec{S}_1^{(n,m)} & \vec{S}_2^{(n,m)} & \cdots & \vec{S}_k^{(n,m)} \\ | & | & \cdots & | \end{pmatrix} \tag{13}$$

Optics EXPRESS

The Mueller matrix $\tilde{M}_{(n,m)}$ associated with diffraction order (n, m) is given by:

$$\tilde{M}_{(n,m)}\tilde{C} = \tilde{O}_{(n,m)} \tag{14}$$

$$\tilde{M}_{(n,m)} = \tilde{O}_{(n,m)}\tilde{C}^T(\tilde{C}\tilde{C}^T)^{-1} \tag{15}$$

Each Mueller matrix is then further post processed, to get the desired polarization properties: to get the retardance and diattenuation properties from a Mueller matrix, we use the polar decomposition analogue for the Mueller calculus, known as the Lu-Chipman decomposition [36], after which we can extract out the retardance, diattenutation, and their respective eigen-axes.

While showing working devices at the visible wavelength using TiO_2 metasurfaces is important from a technological standpoint, note, that the design principle discussed is wavelength-agnostic, and thus could be useful for any suitable material choice at a desired wavelength. Furthermore, the limitation of our metasurface platform (i.e each pillar can only do a unitary and symmetric transformation) in the context of our work, is discussed in detail in Supplement 1.

3. Results

As proof of concept, we design, fabricate, and measure five different 2D metasurface diffraction gratings with different polarization responses in the first eight diffraction orders, $\{G\} = \{(0, 1), (1, 1), (1, 0), (1, -1), (0, -1), (-1, -1), (-1, 0), (-1, 1), (0, 1)\}$. The fabricated metasurfaces are designed for an incident wavelength $\lambda = 532$nm and normal incidence. We show the results of three out of five gratings, here in the main text, while the remaining are shown in Supplement 1. The designs chosen are arbitrary, but they are representative of what can, in general, be achieved in the polarization optics design space, while employing the techniques and technology used in this work.

We have compiled results for three of the gratings in Figs. 4–6. Note that we show ideal, simulated, and measured, juxtaposed for comparison. The ideal refers to the results of our numeric optimization, in which the designed Jones matrices are accurate to a set tolerance of four decimal places. (Thus the numerical polarization responses could be considered 'perfect' from a practical standpoint). This degree of accuracy in polarization response comes at the cost of overall device efficiency. As you can note in Fig. 4, each order has an ideal (numerical) diffraction efficiency of 8.88%, which means the overall numerical efficiency of the grating is $8 \times 8.88\% \simeq 71\%$. The rest of the power is lost to extraneous orders of diffraction, which are actually necessary to afford our optimization the flexibility to meet design requirements. The presence of these extraneous orders of diffraction as loss channels can also be understood as a consequence of having more tuning parameters in the design space. In our case, the grating period consists of 11×11 nanopillars, but increasing the parameter space with the addition of more pillars (pillar separation is fixed at 420nm), would also increase the period of the grating, resulting in more orders of diffraction available for the light to leak into. The focus of our work, is achieving the desired polarization responses, and relative powers between orders, rather than getting a high absolute efficiency. The latter while important, is not a necessary requirement for most polarization optics applications because often one can increase the incident power externally. The simulated responses refer to the results compiled from FDTD simulations, using actual ellipsometry TiO_2 data, and the optimized device dimensions. The measured responses refer to the results compiled following full-Stokes polarimetry of fabricated devices. Note that error bars have not been included, as errors are separately discussed in Fig. 7.

Figure 4 shows the result of a 'diattenuator-only' grating, where we only engineer the diattenuation property of the polarization transformation, in the orders of interest, while avoiding any retardance (in which case the retardance part of the transformation is simply the identity matrix). In this specfic design, in the orders of interest $\{G\}$, the diattenutation changes from 1 (full-contrast), to 0.5 (partial contrast), to 0 (no contrast), and the diattenuation-axes are

Optics EXPRESS

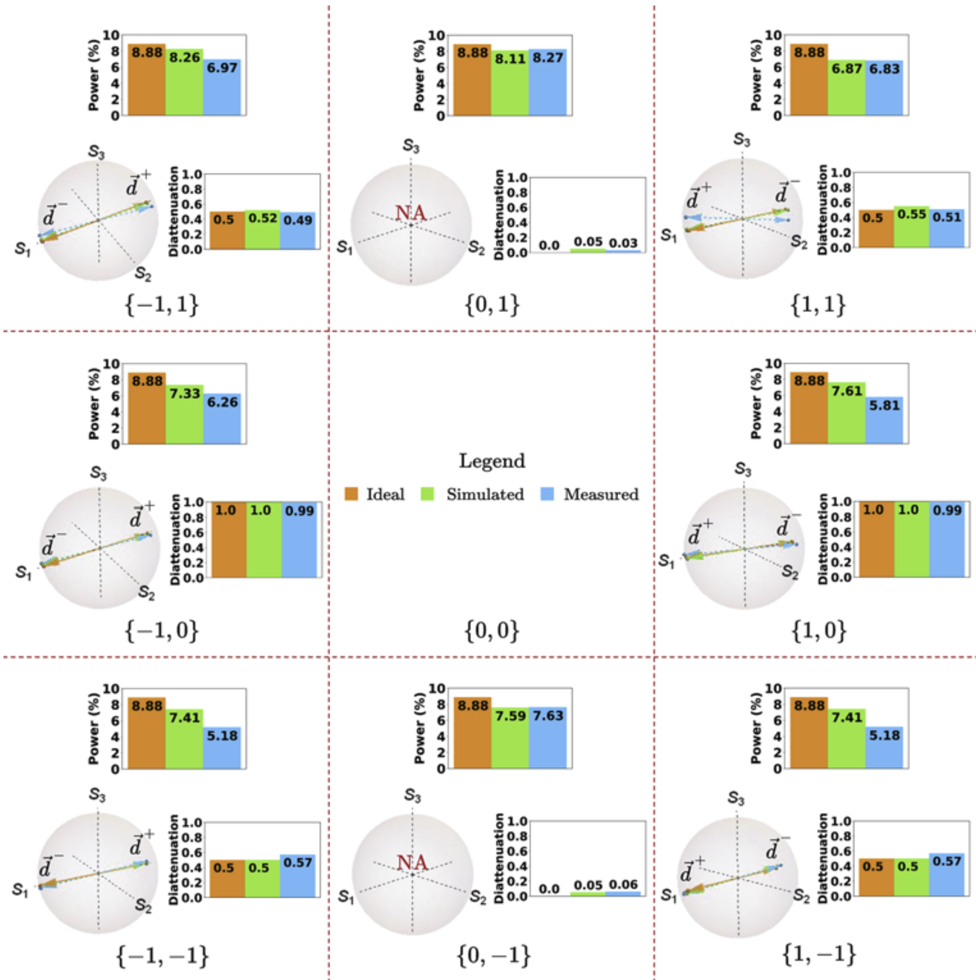

Fig. 4. Far-field results of a 2D metasurface diffraction grating with varying diattenuation. In this grating, the diattenuation values of the designed Jones matrix responses, change, across the eight orders of interest, while the diattenuation-axes are designed to be symmetric, i.e $\vec{d}^+$ is aligned along S_1 axis for half the orders, and anti-aligned for the other half. The diattenuation-axes are plotted on the Poincaré sphere.

designed such that the maximum transmission axis is aligned along S_1 for half the orders, and is anti-aligned for the other half. Another example of a 'diattenuator-only' grating is seen in Fig. S2 in Supplement 1, in which we keep the same diattenuation, but change the diattenuation-axes across orders of interest.

Figure 5 shows the results of a 'retarder-only' grating, where we only engineer the retardance property of the polarization transformation, in the orders of interest, while avoiding any diattenuation (in which case the diattenuation part of the transformation is simply the identity matrix). In this specfic design, in the orders of interest $\{G\}$, the retardance is kept at a constant of 90° (quarter-wave), while the retardance-axes is designed to rotate along the S_1-S_2 plane of the Poincaré sphere, in fixed increments of 45°, as we move from one order in $\{G\}$ to another. Another example of a 'retarder-only' grating is seen in Fig. S3 in Supplement 1, in which we keep the same retardance-axes, but change the retardance values, across orders of interest.

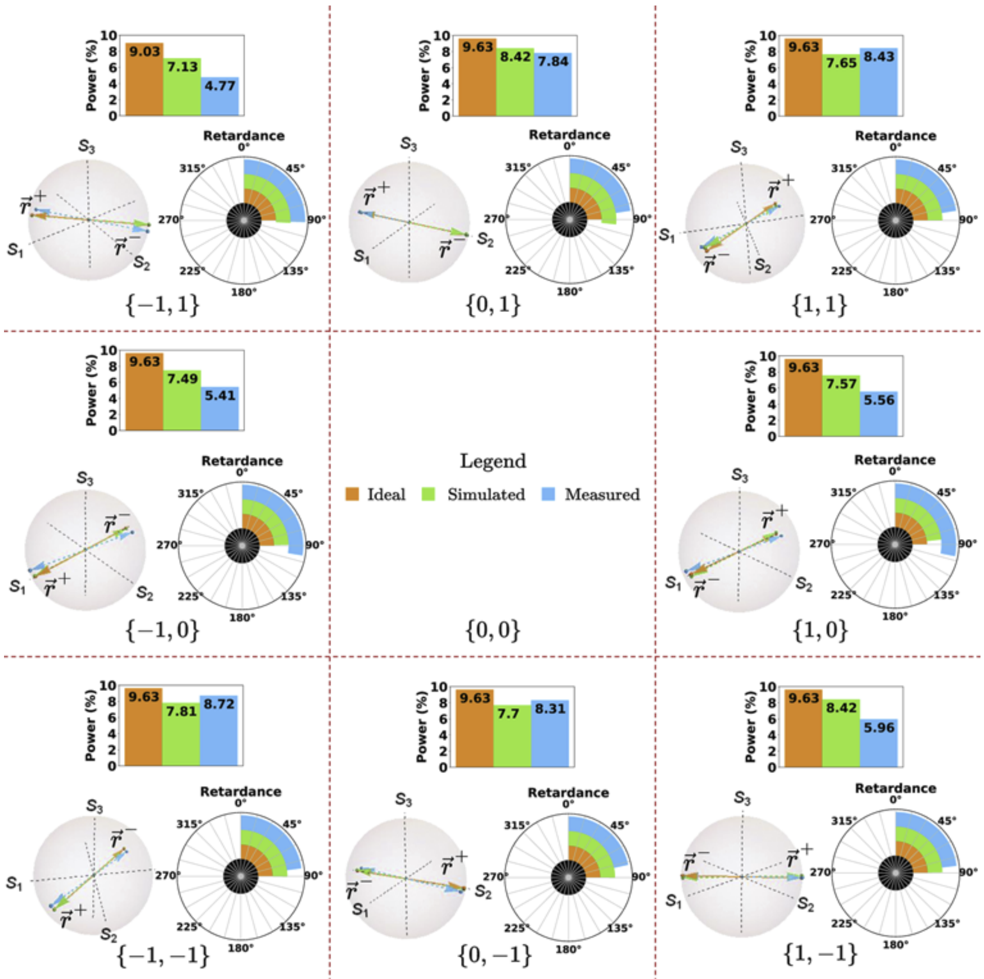

Fig. 5. Far-field results of a 2D metasurface diffraction grating with varying retardance-axes. In this grating, the retardance values of the designed Jones matrix responses, are kept the same ($R = 90°$), while the retardance axes are designed to rotate, across the eight orders of interest. The retardance-axes are plotted on the Poincaré sphere, and the retardance-axes rotate along the S_1-S_2 plane.

Figure 6 shows the results of a 'general' polarization grating, in which we simultaneously engineer the diattenuation and retardance properties in orders of interest $\{G\}$. As we move from one order to another, we see that the diattenuation, and retardance values, as well as their respective eigen-axes are designed to change arbitrarily, showing the flexibility and versatility of our optimization-enabled design space.

Note that the results shown Figs. 4–6 are not snapshot measurements, but are in fact, time-averaged. The error bars associated with the time-averaged measurements have not been included, after they were found to be negligible. This is unsurprising, given that our setup was fully automated, and that the commercial polarimeter (ThorLabs model PAX5710VIS-T) measures Stokes components within an accuracy of 0.5%. A more meaningful error metric is the difference between the designed/desired polarization properties, and the ones ultimately measured after fabricating the device, results of which are compiled in Fig. 7. Another interesting value to consider is the depolarization index [2] – which is the degree of resulting depolarization –

Optics EXPRESS

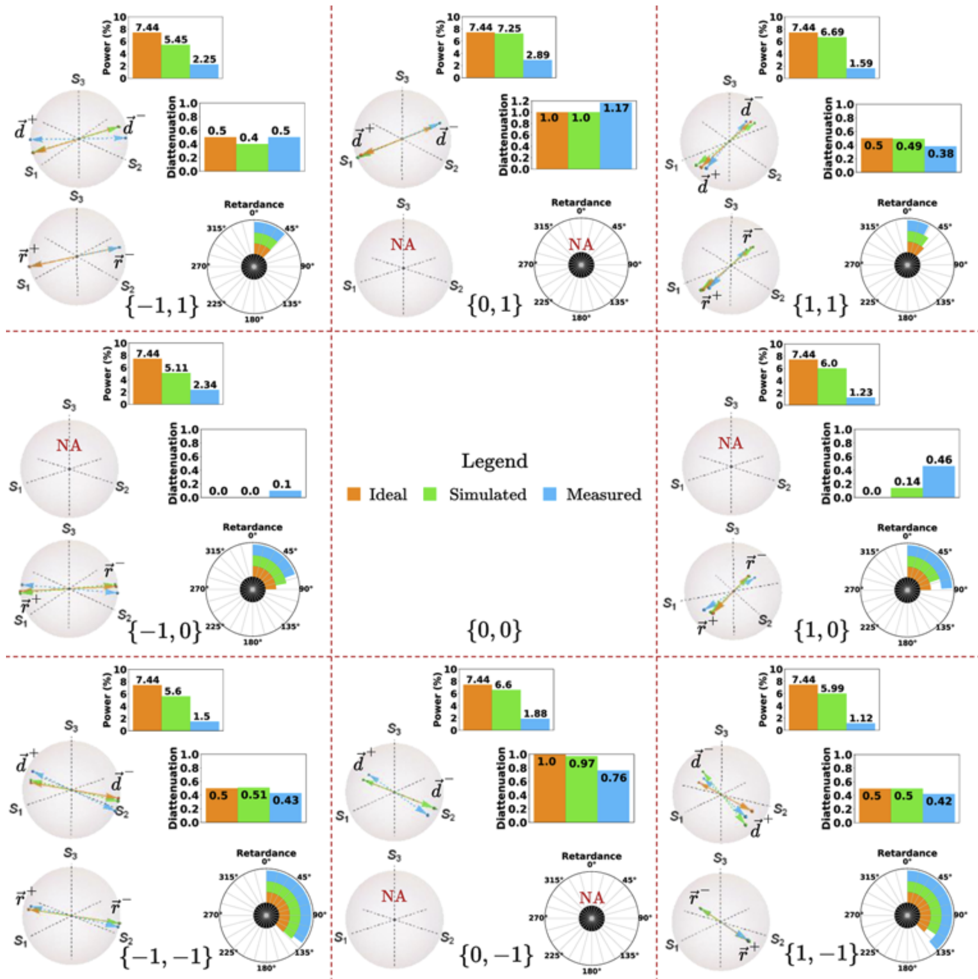

Fig. 6. Far-field results of a 2D metasurface diffraction grating with varying diattenuation and retardances properties. In this grating, the diattenuation, the diattenuation-axes, the retardance, and the retardance-axes, all change across orders of interest. The axes are plotted on the Poincaré sphere, and the axes rotate along the S_1-S_2 plane.

results of which are shown in Fig. 7(c). During our data analysis process, we can compute the depolarization index, from the Mueller matrix, at each grating order of interest. For a non-depolarizing system, the depolarization index should be 1. Since the laser we use is coherent over the length scales of our measurement, and there are no other sources of depolarization in the setup, our system always has a depolarization index of 1, for all diffraction orders. This measure provides us with a good sanity check: if our measurement setup (including alignment of the polarimeter etc) and analysis is correct, then the computed depolarization index for each diffraction order should be ~ 1. Any random or systematic error during measurement, could potentially show up as an artifact of depolarization with a depolarization index $\neq 1$. As we see in Fig. 7(c), the mean depolarization index is well position at ~ 1.01 with a standard deviation of $\sim 4\%$, which shows that our measurements are robust.

Optics EXPRESS

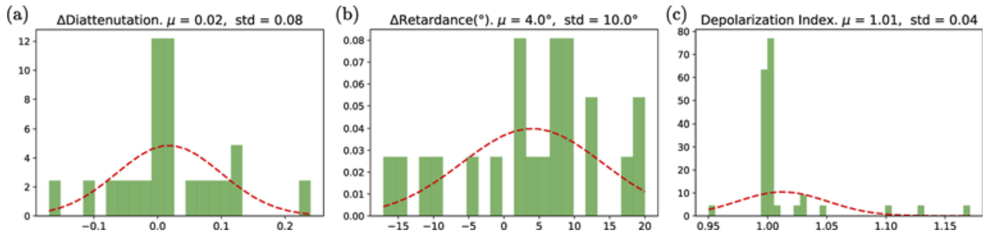

Fig. 7. Histograms of the measured Δ diattenuation, Δ retardance, and depolarization index. (a) The diattenuations measured across various devices and their diffraction orders, show that the standard deviation in the measured diattenuations with respect to the desired diattenuations is $\sim$ 8%. (b) The retardances measured across various devices and their diffraction orders, show that the standard deviation in the measured retardances with respect to the desired retardances is $\sim 10^\circ$. (c) The depolarization index, which should ideally be 1 because there is no inherent depolarization in the system, is well poised at a mean $\mu = 1.01$ with a standard deviation of $\sim$ 4%.

4. Discussion

We have shown, how to design a multi-order device with simultaneous control over the polarization properties. The design strategy can implement any conceivable polarization transformation on the diffraction orders, using phase-only structures such as metasurfaces. One inherent limitation of using linearly birefringent metasurfaces is that one is confined to designing symmetric Jones matrices in the far-field. This limitation is discussed in detail in Supplement 1. However, note that this is only a limitation of our specific platform, and not a fundamental one, since our optimization scheme does allow for the implementation of any 2×2 Jones matrix. Our work also focuses on completely polarized light, fully characterized by Jones calculus, which is suitable for many current applications. A more complete treatment, however, would involve partial polarization and depolarization, which can potentially be introduced in the system via spatial incoherence [37], and would be subject of future work.

It is also important to discuss the inability of conventional polarization optics, such as quater/half waveplates and polarizers, to realize arbitrary Jones matrix transformations. While it is possible to engineer an arbitrary retardance transformation – by either custom-cutting a waveplate to a thickness that corresponds to the desired retardance, or by cascading quarter and half wave plates – it is much harder to engineer an arbitrary diattenuation transformation, using off-the-shelf solutions, such as polarizers and waveplates. Instead of cumbersome conventional solutions, the single metasurface device we propose in this work can be used to perform, not just one, but a set of arbitrary transformations on multiple orders. In the future, the novel way of designing polarization optics introduced in this work, will help replace bulky conventional polarizers and waveplates, especially in applications requiring compact designs. The finer control over diattenutations and retardances shown in our work should also open up possibilities beyond standard polarization optics. Furthermore, recent advances in multi-wavelength [38] and broadband metasurfaces [39,40] should allow the implementation of our work over a broad band of frequencies, which would be much more useful in practical settings.

One area of particular interest is that of polarization aberrations [34]. Polarization aberrations are deviations from a uniform polarization state expected in an optical system [2]. Parasitic diattenuation and retardance in an optical system can unwittingly transform the expected or desired polarization state within an optical system. This can be undesirable in a number of applications. For instance, the point spread function (PSF) of astronomical telescopes depends not only on geometric abberations, but also on polarization dependent abberations introduced by reflection and transmission through various coatings within the optical system [41]. While

Optics EXPRESS

the polarization abberations may appear small in scale, the effect is enough to interfere with the detection of large stellar bodies such as exoplanets [42]. Polarization abberations have also been a problem in polarized-light microscopy, where simultaneously achieving high spatial resolution and contrast is hard because of the presence of these polarization abberations [43]. Their correction is thus paramount in such optical systems. The flexibility in engineering diattenutation and retardance properties in our devices, open up a potentially exciting area of research in countering parasitic polarization aberrations in any optical or imaging system, using custom designed metasurfaces. Investigating the uses of metasurface polarization gratings in overcoming polarization abberations, would be subject of future work.

Funding. National Science Foundation (1541959); Air Force Office of Scientific Research (FA9550-19-0135).

Acknowledgments. A.Z and N.A.R developed the theoretical framework. A.Z performed the optimization and simulation of designs. A.Z, N.A.R and J.S.P fabricated the devices. A.Z meaured the devices with assistance from A.H.D. A.Z analyzed the data. A.Z and F.C wrote the manuscript. F.C supervised the project. J.S.P. is on leave from the Korea Institute of Science and Technology.

Disclosures. The authors declare no competing interests.

Data availability. Data underlying the results presented in this paper are not publicly available at this time but may be obtained from the authors upon reasonable request.

Supplemental document. See Supplement 1 for supporting content.

References

1. W. Shurcliff, *Polarized Light: Production and Use* (Harvard University, 1962).
2. R. A. Chipman, W.-S. T. Lam, and G. Young, *Polarized Light and Optical Systems* (CRC Press, 2019).
3. D. H. Goldstein, *Polarized Light* (CRC Press, 2010) 3rd ed.
4. R. Hegedüs, S. Åkesson, R. Wehner, and G. Horváth, "Could Vikings have navigated under foggy and cloudy conditions by skylight polarization? On the atmospheric optical prerequisites of polarimetric Viking navigation under foggy and cloudy skies," Proc. R. Soc. A **463**(2080), 1081–1095 (2007).
5. C. Brosseau, "Chapter 3 - Polarization and Coherence Optics: Historical Perspective, Status, and Future Directions," Prog. Opt. **54**, 149–208 (2010).
6. J. N. Damask, *Polarization Optics in Telecommunications* (Springer, 2005).
7. A. Yariv and P. Yeh, *Photonics: Optical Electronics in Modern Communications* (Oxford University, 2006).
8. S. J. Wiktorowicz and G. P. Laughlin, "Toward the detection of exoplanet transits with polarimetry," The Astrophys. J. **795**(1), 12 (2014).
9. J. O. Stenflo, "Instrumentation for Solar Polarimetry," in Solar Magnetic Fields: Polarized Radiation Diagnostics, (Springer Netherlands, Dordrecht, 1994), pp. 312–350.
10. P. Y. Deschamps, J. C. Buriez, F. M. Bréon, M. Leroy, A. Podaire, A. Bricaud, and G. Sèze, "The POLDER mission: instrument characteristics and scientific objectives," IEEE Transactions on Geosci. Remote. Sens. **32**(3), 598–615 (1994).
11. T. Novikova, A. Pierangelo, and A. De Martino, "Polarimetric imaging for cancer diagnosis and staging," Opt. Photonics News **23**(10), 26–33 (2012).
12. A. Pierangelo, A. Nazac, A. Benali, P. Validire, H. Cohen, T. Novikova, B. H. Ibrahim, S. Manhas, C. Fallet, M.-R. Antonelli, and A. De Martino, "Polarimetric imaging of uterine cervix: a case study," Opt. Express **21**(12), 14120–14130 (2013).
13. J. S. Tyo, D. L. Goldstein, D. B. Chenault, and J. A. Shaw, "Review of passive imaging polarimetry for remote sensing applications," Appl. Opt. **45**(22), 5453–5469 (2006).
14. F. Snik, J. Craven-Jones, M. Escuti, S. Fineschi, D. Harrington, A. De Martino, D. Mawet, J. Riedi, and J. S. Tyo, "An overview of polarimetric sensing techniques and technology with applications to different research fields," Proc. SPIE **9099**, 90990B (2014).
15. M. Born and E. Wolf, *Principles of Optics* (Pergamon, 1999).
16. Y.-H. Kim, S. P. Kulik, and Y. Shih, "Quantum teleportation of a polarization state with a complete bell state measurement," Phys. Rev. Lett. **86**(7), 1370–1373 (2001).
17. M. Gündoğan, P. M. Ledingham, A. Almasi, M. Cristiani, and H. de Riedmatten, "Quantum storage of a photonic polarization qubit in a solid," Phys. Rev. Lett. **108**(19), 190504 (2012).
18. D. Lin, P. Fan, E. Hasman, and M. L. Brongersma, "Dielectric gradient metasurface optical elements," Science **345**(6194), 298–302 (2014).
19. G. Zheng, H. Mühlenbernd, M. Kenney, G. Li, T. Zentgraf, and S. Zhang, "Metasurface holograms reaching 80% efficiency," Nat. Nanotechnol. **10**(4), 308–312 (2015).
20. R. C. Devlin, M. Khorasaninejad, W.-T. Chen, J. Oh, and F. Capasso, "Broadband high-efficiency dielectric metasurfaces for the visible spectrum," Proc. Natl. Acad. Sci. **113**(38), 10473–10478 (2016).

21. N. Yu, P. Genevet, M. A. Kats, F. Aieta, J. P. Tetienne, F. Capasso, and Z. Gaburro, "Light propagation with phase discontinuities: generalized laws of reflection and refraction," Science **334**(6054), 333–337 (2011).
22. A. Arbabi, Y. Horie, M. Bagheri, and A. Faraon, "Dielectric metasurfaces for complete control of phase and polarization with subwavelength spatial resolution and high transmission," Nat. Nanotechnol. **10**(11), 937–943 (2015).
23. J. P. B. Mueller, N. A. Rubin, R. C. Devlin, B. Groever, and F. Capasso, "Metasurface polarization optics: independent phase control of arbitrary orthogonal states of polarization," Phys. Rev. Lett. **118**(11), 113901 (2017).
24. M. Khorasaninejad, W. T. Chen, A. Y. Zhu, J. Oh, R. C. Devlin, D. Rousso, and F. Capasso, "Multispectral chiral imaging with a metalens," Nano Lett. **16**(7), 4595–4600 (2016).
25. B. Groever, N. A. Rubin, J. P. B. Mueller, R. C. Devlin, and F. Capasso, "High-efficiency chiral meta-lens," Sci. Rep. **8**(1), 7240 (2018).
26. J. A. Davis, I. Moreno, M. M. Sánchez-López, K. Badham, J. Albero, and D. M. Cottrell, "Diffraction gratings generating orders with selective states of polarization," Opt. Express **24**(2), 907–917 (2016).
27. N. A. Rubin, A. Zaidi, M. Juhl, R. P. Li, J. P. B. Mueller, R. C. Devlin, K. Leósson, and F. Capasso, "Polarization state generation and measurement with a single metasurface," Opt. Express **26**(17), 21455–21478 (2018).
28. E. Arbabi, S. M. Kamali, A. Arbabi, and A. Faraon, "Vectorial Holograms with a Dielectric Metasurface: Ultimate Polarization Pattern Generation," ACS Photonics **6**(11), 2712–2718 (2019).
29. R. Zhao, B. Sain, Q. Wei, C. Tang, X. Li, T. Weiss, L. Huang, Y. Wang, and T. Zentgraf, "Multichannel vectorial holographic display and encryption," Light: Sci. Appl. **7**(1), 95 (2018).
30. N. A. Rubin, G. D'Aversa, P. Chevalier, Z. Shi, W. T. Chen, and F. Capasso, "Matrix Fourier optics enables a compact full-Stokes polarization camera," Science **365**(6448), eaax1839 (2019).
31. G. Xu, G. V. Eleftheriades, and S. V. Hum, "Discrete-fourier-transform-based framework for analysis and synthesis of cylindrical Omega-bianisotropic metasurfaces," Phys. Rev. Appl. **14**(6), 064055 (2020).
32. M. Masyukov, A. N. Grebenchukov, A. V. Vozianova, and M. K. Khodzitsky, "Bilayer terahertz chiral metasurfaces with different dihedral symmetries," J. Opt. Soc. Am. B **38**(2), 428–434 (2021).
33. M. Kang, K. M. Lau, T. K. Yung, S. Du, W. Y. Tam, and J. Li, "Tailor-made unitary operations using dielectric metasurfaces," Opt. Express **29**(4), 5677–5686 (2021).
34. J. P. M. Jr and R. A. Chipman, "Polarization Aberrations In Optical Systems," in *Current Developments in Optical Engineering II*, vol. 0818 R. E. Fischer and W. J. Smith, eds., International Society for Optics and Photonics (SPIE, 1987), pp. 240–257.
35. L. Romero and F. Dickey, "Mathematical aspects of laser beam shaping and splitting," in International Optical Design Conference and Optical Fabrication and Testing, (Optical Society of America, 2010), p. IWC3.
36. S.-Y. Lu and R. A. Chipman, "Interpretation of Mueller matrices based on polar decomposition," J. Opt. Soc. Am. A **13**(5), 1106–1113 (1996).
37. A. Lizana, I. Estévez, F. A. Torres-Ruiz, A. Peinado, C. Ramirez, and J. Campos, "Arbitrary state of polarization with customized degree of polarization generator," Opt. Lett. **40**(16), 3790–3793 (2015).
38. Z. Shi, M. Khorasaninejad, Y.-W. Huang, C. Roques-Carmes, A. Y. Zhu, W. T. Chen, V. Sanjeev, Z.-W. Ding, M. Tamagnone, K. Chaudhary, R. C. Devlin, C.-W. Qiu, and F. Capasso, "Single-layer metasurface with controllable multiwavelength functions," Nano Lett. **18**(4), 2420–2427 (2018).
39. W. T. Chen, A. Y. Zhu, V. Sanjeev, M. Khorasaninejad, Z. Shi, E. Lee, and F. Capasso, "A broadband achromatic metalens for focusing and imaging in the visible," Nat. Nanotechnol. **13**(3), 220–226 (2018).
40. W. T. Chen, A. Y. Zhu, J. Sisler, Z. Bharwani, and F. Capasso, "A broadband achromatic polarization-insensitive metalens consisting of anisotropic nanostructures," Nat. Commun. **10**(1), 355 (2019).
41. J. P. McGuire and R. A. Chipman, "Diffraction image formation in optical systems with polarization aberrations. i: Formulation and example," J. Opt. Soc. Am. A **7**(9), 1614–1626 (1990).
42. R. A. Chipman, W. S. T. Lam, and J. Breckinridge, "Polarization aberration in astronomical telescopes," in *Polarization Science and Remote Sensing VII*, vol. 9613 J. A. Shaw and D. A. LeMaster, eds., International Society for Optics and Photonics (SPIE, 2015), pp. 124–134.
43. E. W. Hansen, "Overcoming Polarization Aberrations In Microscopy," in *Polarization Considerations for Optical Systems*, vol. 0891 R. A. Chipman, ed., International Society for Optics and Photonics (SPIE, 1988), pp. 190–203.